

12

Report SAM-TR-82-25

AD A122226

OCULAR THERMAL INJURY FROM INTENSE LIGHT

Ralph G. Allen, Ph.D.

Garrett D. Polhamus, Captain, USAF

DTIC
DEC 9 1982
H

September 1982

Final Report for Period June 1981 - March 1982

Approved for public release; distribution unlimited.

USAF SCHOOL OF AEROSPACE MEDICINE
Aerospace Medical Division (AFSC)
Brooks Air Force Base, Texas 78235



DTIC FILE COPY

92 12 09 016

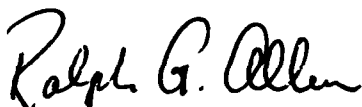
NOTICES

This final report was prepared by personnel of the Laser Effects Branch, Radiation Sciences Division, USAF School of Aerospace Medicine, Aerospace Medical Division, AFSC, Brooks Air Force Base, Texas, under job order 7757-02-51.

When U.S. Government drawings, specifications, or other data are used for any purpose other than a definitely related Government procurement operation, the Government thereby incurs no responsibility nor any obligation whatsoever; and the fact that the Government may have formulated, furnished, or in any way supplied the said drawings, specifications, or other data is not to be regarded by implication or otherwise, as in any manner licensing the holder or any other person or corporation, or conveying any rights or permission to manufacture, use, or sell any patented invention that may in any way be related thereto.

This report has been reviewed by the Office of Public Affairs (PA) and is releasable to the National Technical Information Service (NTIS). At NTIS, it will be available to the general public, including foreign nations.

This technical report has been reviewed and is approved for publication.



RALPH G. ALLEN, Ph.D.
Project Scientist



GARY W. WEST, Colonel, USAF, MC
Supervisor



ROY L. DEHART
Colonel, USAF, MC
Commander

20. ABSTRACT (Continued)

validated reasonably well within the limits of their applicability. However, other mechanisms of injury (such as acoustical shock waves, and photochemical interactions) have been identified and have received considerable attention in the past decade. The results of the research efforts of many investigators over a considerable span have been incorporated in numerous laser safety standards, typified by the "American National Standards Institute Z136.1 Standard for the Safe Use of Lasers." These standards, although carefully conceived and based upon a large body of empirical information, are neither complete nor final and should be updated as additional information is obtained.



Accession For	
NTIS GRA&I	<input checked="" type="checkbox"/>
DTIC TAB	<input type="checkbox"/>
Unannounced	<input type="checkbox"/>
Justification	
By	
Distribution/	
Availability Codes	
Dist	Avail and/or Special
A	

CONTENTS

	<u>Page</u>
HISTORY.....	5
RETINAL THERMAL INJURY.....	6
Threshold Retinal Irradiance.....	9
Threshold Temperature.....	12
Temperature and the Damage Integral.....	13
Absorption Coefficients.....	17
Retinal Energy Distribution.....	17
Rate Process Model.....	20
Temperature Measurements.....	22
Blood Flow.....	24
Asymptotic Retinal Thermal Injury.....	24
CORNEAL THERMAL INJURY.....	27
BEYOND THERMAL INJURY.....	36
CONCLUSION.....	37
REFERENCES.....	39

FIGURES

<u>Figure</u> <u>No.</u>		
1.	Schematic diagram of the eye.....	6
2.	Visual acuity distribution at the retina.....	7
3.	Typical circular thermal retinal lesions (Photo).....	8
4.	Characteristics of circular thermal retinal lesions.....	10
5.	Threshold retinal exposure for visible lesions in the rhesus monkey	11
6.	Typical temperatures predicted by the model.....	14
7.	Typical temperature calculations at different axial positions.....	15
8.	Geometry of heat conduction model of the ocular fundus.....	16
9.	Schematic model of thermal retinal damage.....	16

CONTENTS (Cont'd.)

Figure
No.

10.	Absorption coefficients for rhesus monkey fundus.....	17
11.	Measured images and predicted minimal profiles of intensity for 647-nm laser light.....	21
12.	Temperature-rise history at the image center, normalized with respect to corneal power for a 9.0-sec exposure. Retinal irradiance profile is shown in the insert (Polhamus: Ref. 22).....	22
13.	Radial temperature rise profiles at 9.0 sec, normalized with respect to corneal power (Polhamus: Ref. 22).....	23
14.	Maximum temperature rise at the lesion radius for combined macular and paramacular thresholds for various exposure durations.....	23
15.	Asymptotically predicted threshold temperatures at the lesion radius using the thermal model coupled with the rate process model (Priebe and Welch: Ref. 25).....	25
16.	Temperature increase per joule total intraocular energy vs. exposure duration (Priebe and Welch: Ref. 25).....	26
17.	Normalized temperature for a constant exposure and the point- spread distribution associated with a 6.6-mm pupil diameter (Mainster et al.: Ref 27)	27
18.	Dimensionless temperature vs. dimensionless radial distance for uniform irradiance profile (Priebe and Welch: Ref. 28).....	28
19.	Model predictions for 25- and 10- μ m image diameters compared to experimental observation of a minimum visible lesion of 25 μ m $1/e^2$ diam. (with Henriques' rate constants).....	29
20.	Safety standards for the cornea.....	30
21.	Cornea and lens model geometry (distances in centimeters).....	31
22.	Absorption coefficients for the rhesus ocular media (Maher: Ref. 32).....	31
23.	Comparison of experimental and theoretical (eq. 3) lesion thresholds for three absorption coefficients.....	34
24.	Proposed corneal safety standards (Reed: Ref. 35; and Vos: Ref. 36).	35
25.	Safety standards for the retina.....	36

CONTENTS (Cont'd.)

TABLES

<u>Table No.</u>		<u>Page</u>
1.	Physiological parameters required for optical analysis (Takata et al.: Ref. 10).....	20
2.	Physiological parameters used for clear media analysis (Takata et al.: Ref. 10).....	30
3.	ED ₅₀ values of average power for corneal lesions after exposure to 10.6- μ m radiation.....	33
4.	Bright light sources and some possible consequences to overexposure.....	38

OCULAR THERMAL INJURY FROM INTENSE LIGHT

HISTORY

Ocular injury produced by intense light sources has troubled man for a long time--prime examples of such concern being solar eclipse burns, snow blindness, glassblower's cataracts, and corneal injury from arc welding. Flashblindness from large naval guns has also been a problem to the U.S. Navy. The potential for corneal injury from solar radiation (specifically, the ultraviolet (UV), during extravehicular activities) required NASA to provide the astronauts with helmets with adequate attenuation properties for the lunar landings. The potential for retinal damage and flashblindness from the thermal emissions of nuclear detonations likewise required eye protection for observers at the first detonation in 1945, and studies of retinal injury and flashblindness were undertaken early in the weapons testing program that followed. Concurrently, Meyer and Schwickerath developed the Zeiss Xenon Photo-coagulator for treatment of eye disorders, particularly, detached retinae and diabetic retinopathy. Currently, the Argon laser is a very effective light source in the treatment of such retinal problems.

About the mid-1950's, systematic laboratory studies of chorioretinal burns began, at the USAF School of Aerospace Medicine (USAFSAM) and at the Medical College of Virginia under Air Force contract. The purpose of these studies was to explore the eye hazards associated with nuclear detonations. The subjects were rabbits, and a Zeiss Photocoagulator was the source. The primary endpoint in these early studies was a "minimum" visible retinal lesion, with a threshold generally identified as the average of the lowest retinal irradiance that produced a visible lesion, and the highest retinal irradiance that did not produce a visible lesion--within 5 min. Also considered were such factors as image size, blood flow, ocular transmission, enzyme inactivation, and light microscopy. In the mid-1960's, the U.S. Air Force, the Defense Atomic Support Agency (DASA), and contractors extended many of these studies to primates (rhesus). Unfortunately, limitations on the radiation sources available prevented systematic examination of spectral effects, exposure durations less than approximately 1 msec, and retinal image sizes less than 75-100 μm . During this period, the primary mechanism for retinal injury was almost universally considered to be thermal, or, for higher exposure levels, the production of a steam bubble or explosion and resultant mechanical trauma.

Shortly after the invention of the Ruby laser in 1961, studies of the biomedical effects of laser radiation were conducted at the Medical College of Virginia and the University of Cincinnati under contracts with the U.S. Army Surgeon General. Soon the U.S. Air Force also began laser effects studies through its Oculo-Thermal Group--later the Laser Effects Branch--at USAFSAM. In large part, the research performed by, or sponsored by, the Department of Defense (DOD) through these Army and Air Force programs was the source of the "American National Standards Institute (ANSI) Z136.1 Laser Safety Standard," which is the basis of the respective laser safety standards for the Armed

Services, and of the "Bureau of Radiological Health (BRH) Laser Product Performance Standard." Although these standards applied primarily to injury to the retina, lens, and cornea, the potential for damage to human skin from intense thermal radiation prompted studies of skin injury and consideration of thermal mechanisms for skin burns.

The complexities of these standards stem directly from: the nature of laser radiation; the kinds of interactions possible between biological tissues and laser radiations; and the range of exposure conditions which can be encountered in the various applications for lasers. Despite the broad scope of current standards, they are based largely on empirical data, and data are still needed in several areas.

RETINAL THERMAL INJURY

Probably the most thoroughly studied mechanism of retinal injury is the "thermal." This injury results from the absorption of energy by the retina and choroid, after the energy has been focused by the cornea and lens. In time, heat generated in the retina and adjacent structures diffuses away from the area in which the image is focused. Heat will also be conducted away by the flow of blood in the vascular bed. If the rate of heat dissipation from an area is less than the rate of heat generation in that area, the temperature will increase. If the temperature exceeds the biologic tolerances for the area involved, then the result will be injury to the photoreceptors (rods and cones), optical nerve tissue, and other structures in the retina and choroid--with possible permanent loss of vision (Fig. 1).

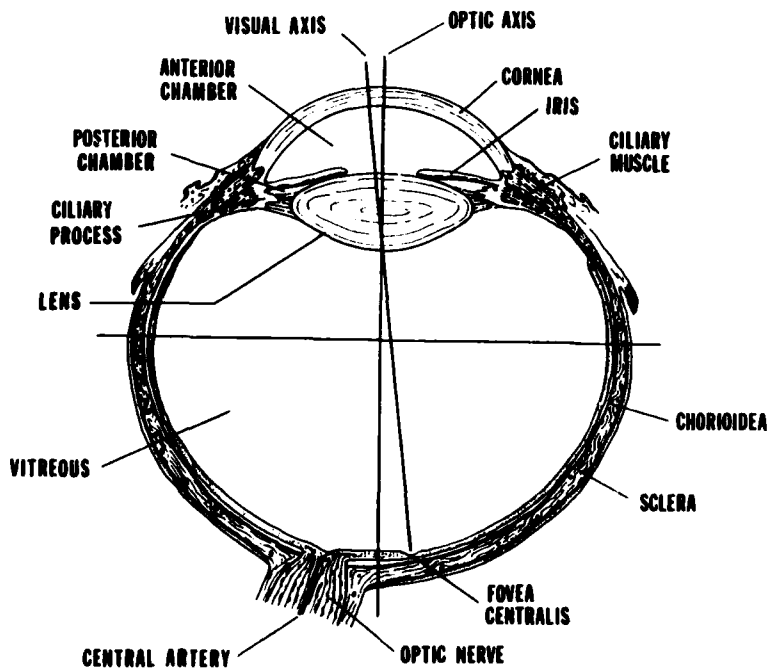


Figure 1. Schematic diagram of the eye.

The degree of visual impairment caused by a retinal burn will be dependent on the size, severity, and location of the lesion. The size of the image, which influences the size of a burn, in general depends on the size and distance of the object from the observer. The severity of a burn depends, in general, upon the amount by which the exposure exceeds the threshold exposure. The location of the burn will determine the function affected. For example, a large burn centered on the fovea will seriously affect visual acuity and color vision. A small burn in the periphery will have significantly less effect on visual acuity and, barring complications, could result in a scotoma or blind spot that would not normally be noticed.

As shown in Figure 2, a burn exactly centered on the fovea and large enough to include the central 2.5-degree visual field would reduce visual acuity to about 57% of normal (20/35 on the Snellen scale). In theory, if the central 10-degree visual field were destroyed, the acuity would be 29% (20/70). If the central 20 degrees of vision were destroyed (an unlikely occurrence), visual acuity would be reduced to approximately 20% (about 20/100). Shown in Figure 3 are typical thermal retinal lesions made by an

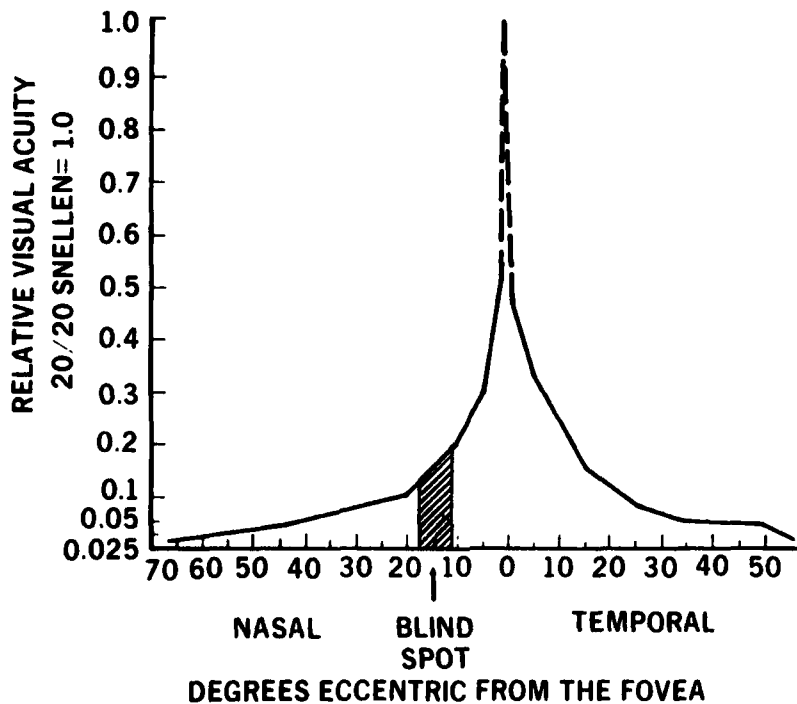


Figure 2. Visual acuity distribution at the retina.

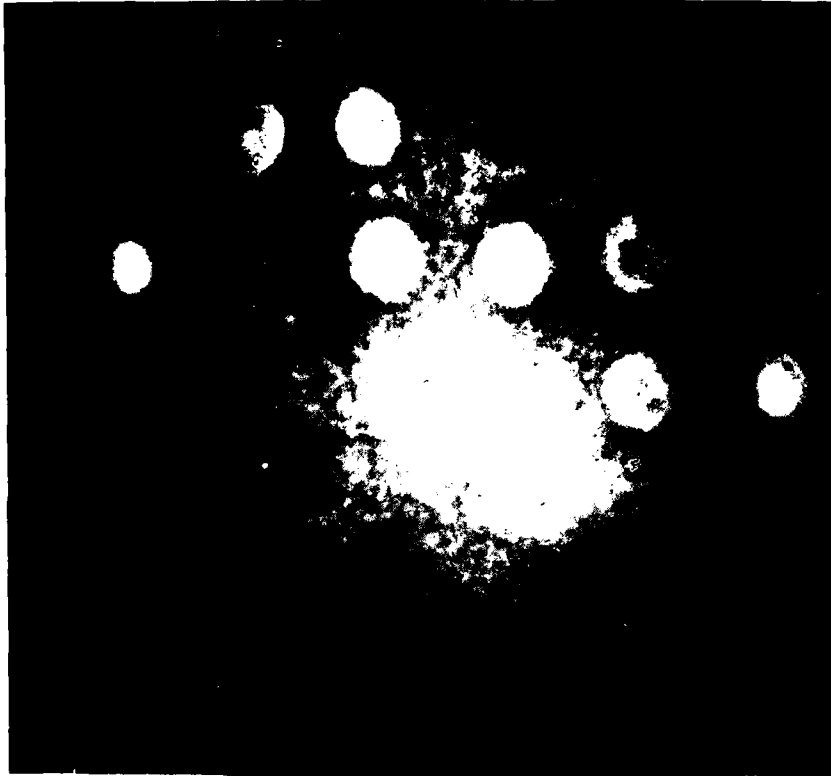


Figure 3. Typical circular thermal retinal lesions.

image of uniform intensity and 0.5 mm in diam., while the typical characteristics of a thermal lesion are illustrated in Figure 4.

Threshold Retinal Irradiance

The prediction model for thermal retinal injury used at USAFSAM by Allen and Richey in 1958--revised and refined in the mid-1960's by Allen (1)--had as its base the early experimental data developed with rabbits as subjects (2). These early data were followed later by primate data (3,4). These experimental data consisted of threshold retinal exposures vs. exposure durations for the production of "minimum" visible lesions viewed with an ordinary ophthalmoscope (Fig. 5). The light sources used in this early work, which preceded the development of lasers, were Zeiss Photocoagulators with infrared radiation above 900 nm filtered out. The experimental results indicated an image-size dependence and, in general, agreed with the widely held view that the mechanism involved in retinal injury was mainly thermal.

For this early prediction model, calculation of the retinal irradiance used the following equation:

$$H_r(t) = \frac{\pi}{[2f(t)]^2} \int_{\lambda_{\min.}}^{\lambda_{\max.}} N_S(\lambda, t) T_A(\lambda) T_E(\lambda) d\lambda \quad (1)$$

where

- $f(t)$ = f number of the eye
- $\lambda_{\min.}, \lambda_{\max.}$ = minimum and maximum wavelengths radiated by the source which reach the retina with energy sufficient to contribute to heating
- t = time
- $N_S(\lambda, t)$ = radiance of the source ($\text{cal}/\text{m}^2\text{-s}$)
- $T_A(\lambda)$ = atmospheric transmission
- $T_E(\lambda)$ = transmission of the clear media of the eye

Integrating the retinal irradiance over the exposure duration yields the retinal exposure:

$$Q_r = \int_0^t H_r(t) dt \quad (2)$$

This prediction model, which simply compared calculated retinal exposures as a function of exposure duration and image size with corresponding measured retinal threshold exposures, still serves well for many situations. However, the empirical basis of this model limits its application to certain classes of exposure conditions, and provides little insight into more complicated exposure conditions.

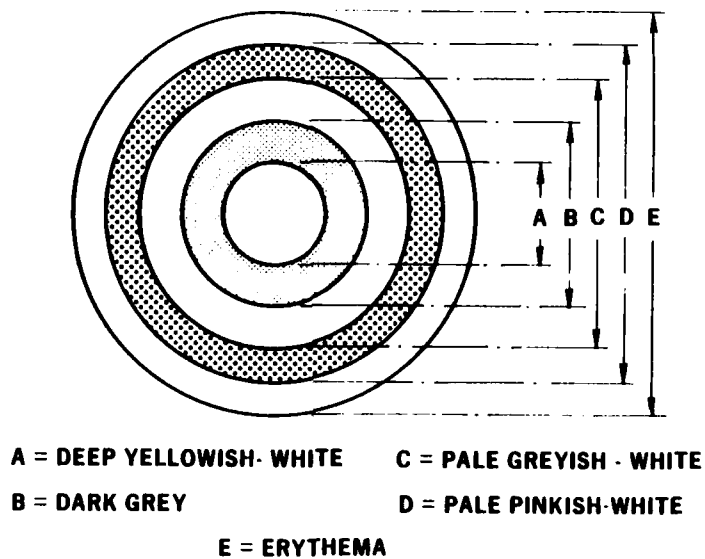


Figure 4. Characteristics of circular thermal retinal lesions.

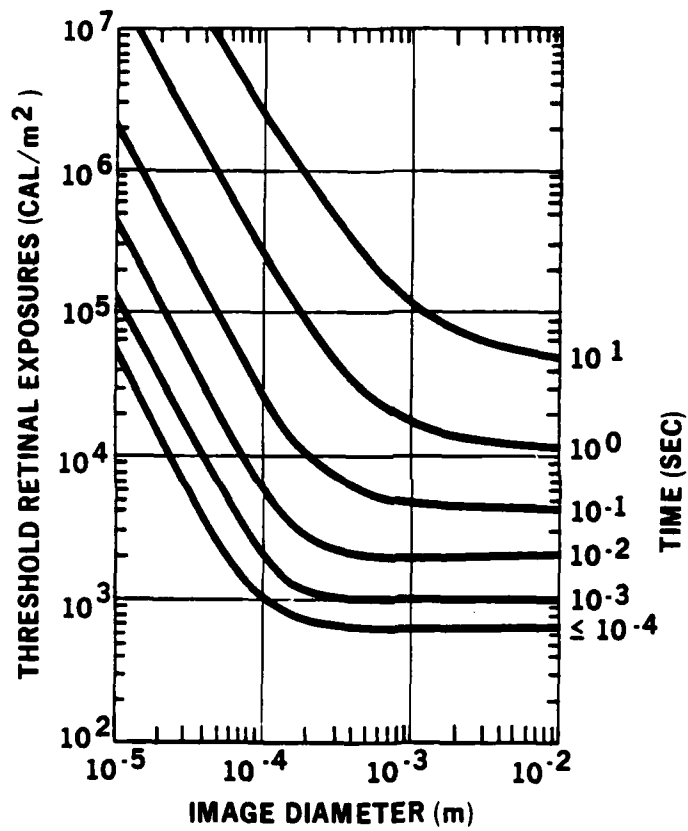


Figure 5. Threshold retinal exposure for visible lesions in the rhesus monkey.

Threshold Temperature

In the early 1960's Wray of DASA (5), and Vos of the Institute for Perception, Netherlands (6), independently developed "temperature" models based on solutions of the heat conduction equation. In cylindrical coordinates, and assuming cylindrical symmetry, this equation takes the form:

$$\frac{\partial T}{\partial t} = \frac{1}{\rho C} S(r,z,t) + \frac{K}{\rho C} \left[\frac{1}{r} \frac{\partial T}{\partial r} + \frac{\partial^2 T}{\partial r^2} \right] + \frac{K}{\rho C} \times \frac{\partial^2 T}{\partial z^2} \quad (3)$$

where

$T(r,z,t)$ = temperature rise ($^{\circ}\text{C}$)

t = time (sec)

ρC = volumetric specific heat ($\text{cal}/\text{cm}^3 - ^{\circ}\text{C}$)

K = thermal conductivity ($\text{cal}/\text{cm} - \text{sec} - ^{\circ}\text{C}$)

and,

$$S(r,z,t) = \int_{\lambda_{\min.}}^{\lambda_{\max.}} h(r) H_0(t,\lambda) \left[- \frac{dX}{dz} (\lambda,z) \right] d\lambda \quad (4)$$

for

$\lambda(\text{min}, \text{max})$ = minimum and maximum wavelengths radiated by the source

$h(r)$ = normalized intensity profile of the image at the retina

$H_0(t,\lambda)$ = center retinal spectral irradiance ($\text{cal}/\text{cm}^2 - \text{sec}$)

$\frac{dX}{dz} (\lambda,z)$ = derivative of the transmission through the tissue (cm^{-1})

Assuming Lambert-Beers absorption, the derivative of the transmission introduces different rates of absorption in the pigment epithelium ($\beta_1(\lambda)$) and choroid ($\beta_2(\lambda)$), as follows:

$$\left[- \frac{dX}{dz} (\lambda,z) \right] = \beta_1(\lambda) e^{-\beta_1(\lambda)z} \quad \text{for the pigment epithelium (P.E.)} \quad (5)$$

and

$$\left[-\frac{dX}{dz}(\lambda, z) \right] = \beta_2(\lambda) e^{d_1(\beta_2(\lambda) - \beta_1(\lambda)) - \beta_2(\lambda)z} \quad (6)$$

for the choroid, where d_1 = thickness of the P.E.
and $z \geq d_1$.

This model provided not only a more satisfying picture of the thermal process produced by the absorption of radiant energy at the retina and choroid, but also the opportunity to examine systematically the more complicated exposure situations. Basically, the model provided a time-history of the volume temperature distribution in the retina and choroid. The solutions represent the temperature rise above an arbitrary ambient temperature. Shown in Figures 6 and 7 is the temperature response from a 20-ms exposure with a disc image 500 μm in diam.

In 1967-1968, Clarke (7) provided a uniform absorption model with an analytical solution to the steady-state diffusion equation. In the early 1970's, the time-dependent temperature model was revised, improved, and adapted to symmetrical noncoherent sources by Mainster et al. (8). Shortly afterwards, Wissler (9) obtained an analytical expression for the transient temperature distribution produced in the retina during laser radiation. His analysis included: tissue layers with different physical properties; energy absorption in the sclera, as well as pigment epithelium (P.E.) and choroid; removal of heat from the tissue by blood circulation; and variation in the light source with time. The results were still limited, however, in that they permitted only the prediction of a time history of temperature distribution, with retinal injury being examined in terms of a maximum-temperature damage criterion.

Temperature and the Damage Integral

In the mid-1970's, Takata et al. (at the Illinois Institute of Technology, Research Institute (10)) revised and generalized the model, adapting it to coherent radiation for the U.S. Air Force. At this point in the evolution of the model, the geometry was as shown in Figure 8.

The model used an exponentially stretched grid in a cylindrical geometry, and variable internal sources and thermal properties. Boundary conditions for equation (3) were:

$$T(R, z, t) = 0,$$

$$T(r, \pm Z, t) = 0,$$

$$T(r, z, 0) = 0.$$

The values of R and Z were equal to 1 cm. The irradiance at the front surface of the P.E. was equal to the radiant energy entering the eye, multiplied by a wavelength-dependent transmission coefficient for the cornea, lens, ocular fluids, and retina.

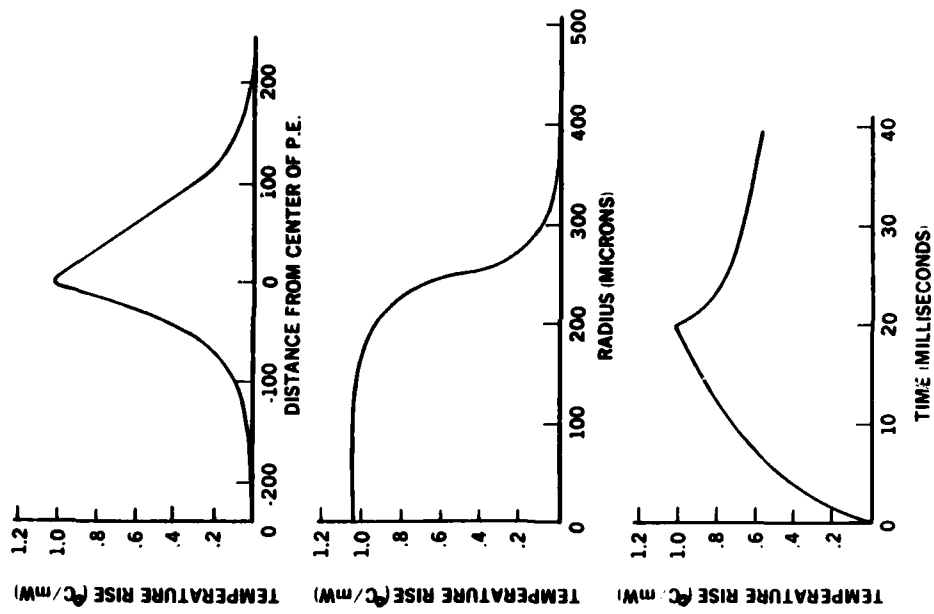


Figure 6. Typical temperatures predicted by the model.

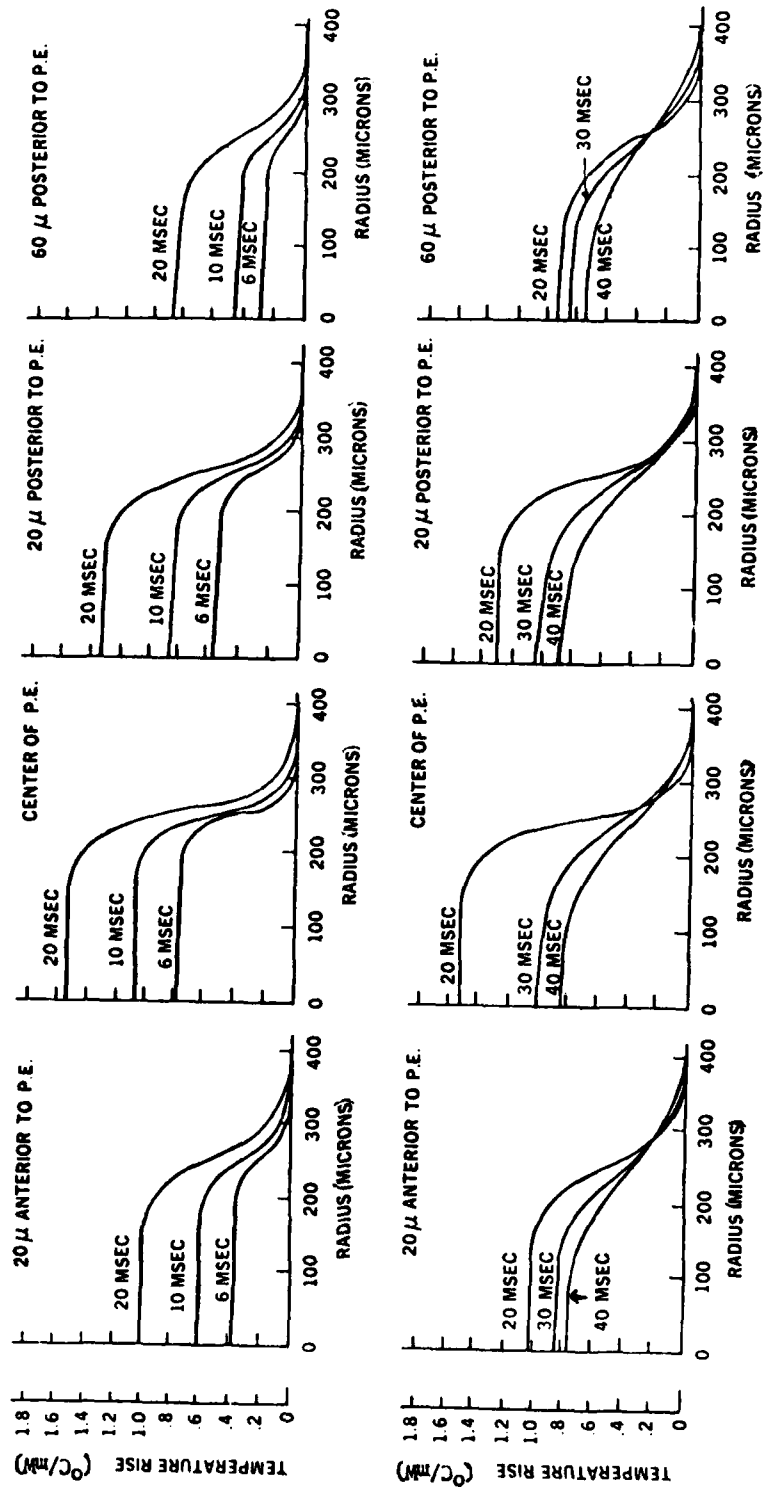


Figure 7. Typical temperature calculations at different axial positions.

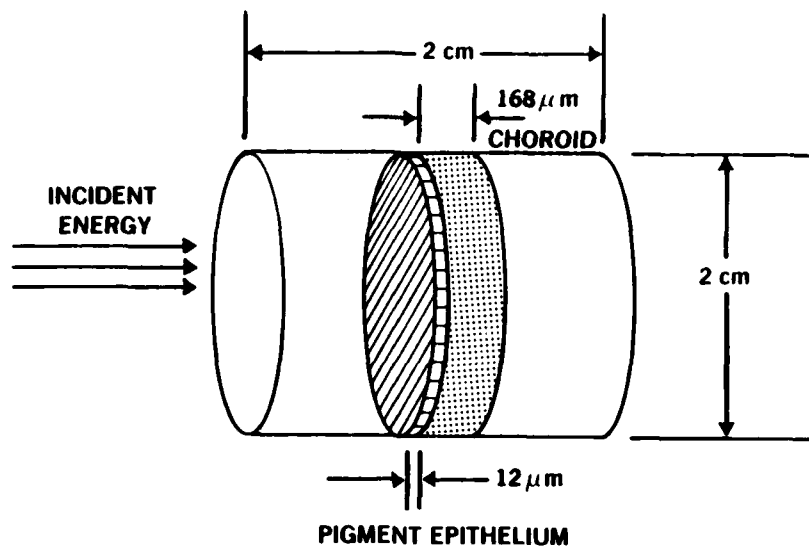


Figure 8. Geometry of heat conduction model of the ocular fundus.

This version of the model had: a heat sink to simulate convection of heat by blood flow; nonuniform absorption in a homogeneous P.E., through absorption by a distribution of discrete pigment granules in the P.E.; and an option to specify the distribution of energy at the retina, or to use a distribution of energy at the retina which approximates that produced by a highly collimated coherent source focused by the eye. In addition, Henriques' damage integral (11) was coupled to the temperature calculation to allow systematic assessment of injury in terms of the temperature rise history (Fig. 9). Emphasized in Figure 9 is the interrelation between the source term, heat conduction, and rate process portions of the model.

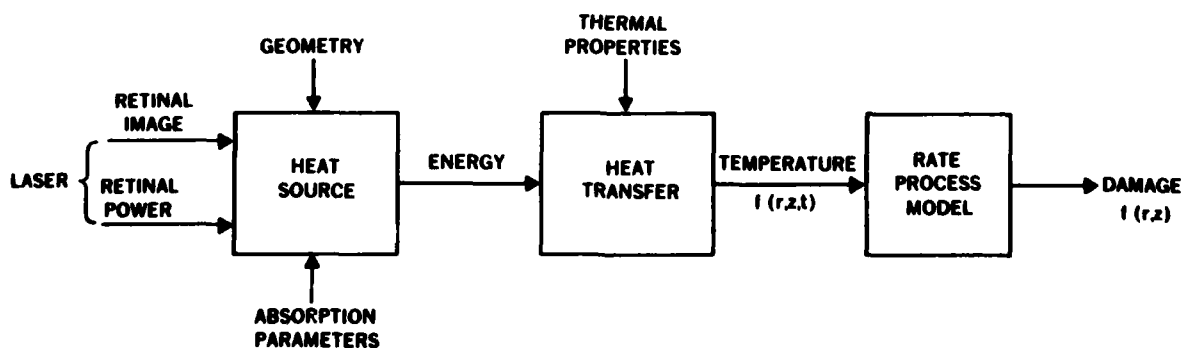


Figure 9. Schematic model of thermal retinal damage.

This model of the thermal mechanism of retinal injury appears adequate for our basic knowledge of the anatomy of the eye, its thermal properties, blood flow, pigment distribution, and absorption coefficients. This is not to say that all of these properties are adequately established--or that the limits of biological variation are known. Questions still exist, in particular, concerning the value of the spectral absorption coefficients of the P.E. and the choroid, the distribution of energy on the retina produced by a highly collimated laser beam, and the values of the rate process damage coefficients.

Absorption Coefficients--Coogan et al. (12) and Gabel et al. (13) provided the only two sets of measured absorption coefficients of the P.E. and separate choroid in rhesus and human retinal tissue (Fig. 10). In the studies of Coogan and Gabel, the thicknesses of the rhesus P.E. samples were, respectively, 12 μm and 4 μm . Choroid thicknesses were approximately equal with a value of 170 μm .

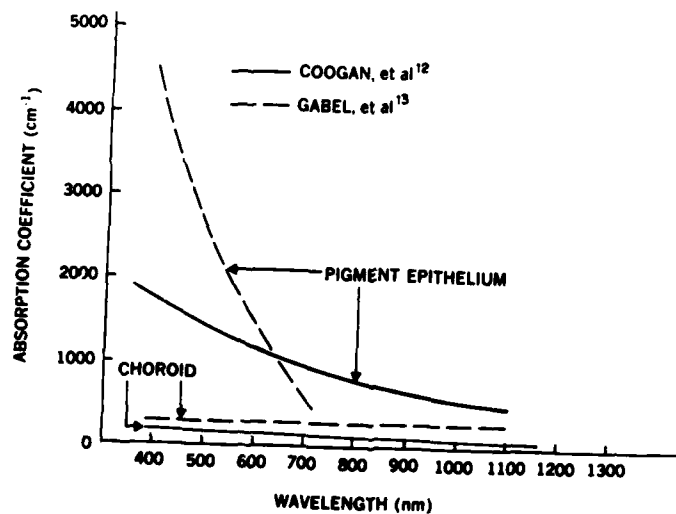


Figure 10. Absorption coefficients for rhesus monkey fundus.

Retinal Energy Distribution--In their version of the model, Takata et al. (10) used the following equation, developed by Weigandt, to calculate the normalized irradiance at the retina:

$$\frac{H(r)}{H(o)} = \left[\frac{1}{\lambda \cdot f'} \int_0^a \sqrt{P_p(\rho)} \cdot J_0 \left(\frac{2\pi \cdot r \cdot \rho}{\lambda \cdot f'} \right) \cdot F_1(\rho) \cdot F_2(\rho) \cdot \rho \, d\rho \right]^2 \quad (7)$$

in which

a = pupil radius (cm)

f' = $f_0 - p$ (cm)

f_0 = second principal focal length at a reference wavelength of λ_0 (cm)

$F_1(\rho)$ = function accounting for defocusing (chromatic and geometric)

$F_2(\rho)$ = function accounting for spherical aberration

J_0 = zero order Bessel function of first kind

p = distance of pupil from second principal plane (cm)

r = radial distance in retinal plane (cm)

λ = wavelength (cm)

ρ = radial distance in pupil plane (cm)

$P_C(R)$ = beam profile at the cornea

$P_p(\rho) = \frac{1}{\phi^2} \times P_C\left(\frac{R}{\phi}\right)$ = profile at pupil plane

where

R = radial distance at cornea

$\phi = 1 - p_C/z_f$

p_C = distance of pupil from cornea

$z_f = n \times z_0 \times f_c / (n \times z_0 - f_c)$, when $n \times z_0 > f_c$

z_C = distance from anterior apex of cornea to image plane in the eye in the absence of the lens

f_C = focal length of cornea.

The functions $F_1(\rho)$ and $F_2(\rho)$ were given by:

$$F_1(\rho) = \exp(i \cdot C_0 \cdot \rho^2) \quad (8)$$

$$F_2(\rho) = \exp(i \cdot C_2 \cdot \rho^4) \quad (9)$$

while the constants C_0 and C_2 were given by:

$$C_0 = \frac{2\pi n}{\lambda \cdot a^2} W = \frac{2\pi n}{\lambda \cdot a^2} [-f' - \Delta z \cdot (1 - \cos\alpha) + (f'^2 - \Delta z^2 \sin^2\alpha)^{1/2}] \quad (10)$$

$$C_2 = -3 \cdot 10^6 / \lambda$$

where

α = angle between the refracted beam at the cornea and the axis of the eye

n = index of refraction at laser wavelength λ

Here, α , Δz , and f can be obtained from the following equations:

$$f = f_0 \cdot n(n_0 - 1) / n_0(n - 1) \quad (11)$$

$$\tan \alpha = a / (f' + \Delta z) \quad (12)$$

$$\Delta z = \frac{n \cdot z_0 \cdot (f/f_0)}{n \cdot (z_0/f_0) - (f/f_0)} - f_0 \quad (13)$$

where

f = focal length at laser's wavelength (cm)

n_0 = index of refraction at a reference wavelength λ_0 (cm)

z_0 = distance of pupil from waist of laser beam (cm)

Constants required for the optical analysis are presented in Table 1 (10). The equation accounts for scalar diffraction (using the Fresnel approximation), spherical aberration, a defocusing function, and chromatic aberration.

TABLE 1. PHYSIOLOGICAL PARAMETERS REQUIRED FOR OPTICAL ANALYSIS
(Takata et al.: Ref.10)

Parameters	Values of parameters (cm)	
	Human eye	Monkey eye
a_{max}	0.35	0.35
f_o (at $\lambda_o = 500$ nm)	2.24	1.68
p	0.135	0.12
f_c	3.12	2.43
p_c	0.31	0.29

Flamant (14) was the first (15,16) to measure the image reflected from the human retina. In the late 1970's, Robson and Enroth-Cugell (17) used a fiber-optic probe to measure the retinal image directly at the retinal plane in anesthetized cats. Soon afterwards, Polhamus and Allen (18) measured the in-vivo irradiance profile in the rhesus monkey eye (Fig. 11). Measurements were made for three laser wavelengths (530, 647, and 1060 nm) and two pupil sizes (2 and 8 mm). For the visible wavelengths, the 1/2-power radii were about 6 μ m, although the images contained significant structure within the profiles.

Rate Process Model--For long duration exposure (1 ms to 10 sec), the most widely used model of thermal tissue damage was the rate process model applied first by Henriques (11) to porcine skin burns. He hypothesized tissue injury caused by the thermal denaturation of protein, and based his model on Arrhenius' reaction rate equation. Johnson et al. (19) examined this equation and the assumptions required for its use in detail. Tissue damage was predicted from the following equation:

$$\Omega(r,z) = A \int_0^t e^{-E/RT(r,z,t)} dt \quad (14)$$

for

A = preexponential constant

E = energy of activation (reflects species sensitivity to heat) (cal/mol)

$T(r,z,t)$ = tissue temperature

R = universal gas constant

Ω = arbitrary criterion for damage (reflects percent of species that is damaged)

With the assumption that radiation produces a step increase in tissue temperature and a step decrease when the exposure stops, equation (14) simplifies to the following:

$$\Omega(r,z) = At_0 e^{-E/RT(r,z,t_0)} \quad (15)$$

where

t_0 = exposure duration(s)

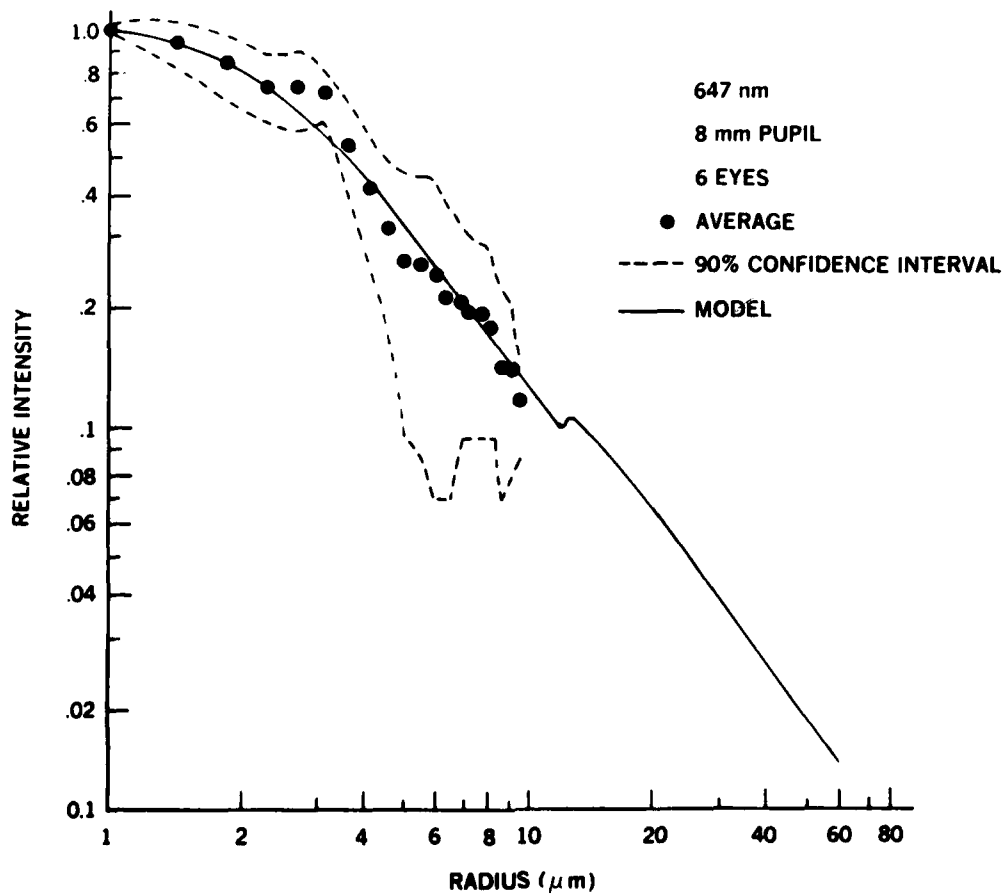


Figure 11. Measured images and predicted minimal profiles of intensity for 647-nm laser light.

Temperature Measurements

To validate the temperature calculations, Cain and Welch (20)--at The University of Texas in Austin--developed microthermocouples especially designed for measuring transient temperatures in tissue. Priebe et al. (21) compared predicted temperatures to measurements in rhesus monkeys for laser exposures of 0.1 - 10 sec. The average ratio of the model temperatures to their measured values was 0.77.

In the late 1970's, at USAFSAM, Polhamus (22) measured retinal temperatures from long-term laser exposures of 9, 100, and 1000 sec; and he compared the measured to the predicted temperatures--measured at the center of the image and at various radial distances (Figs. 12 and 13). The measured temperatures associated with threshold lesions were 15% lower than the predicted temperatures (Fig. 14)--temperatures associated with the lesion radii. Thus, the model predicted the extent of damage reasonably well, despite significant differences between predicted and measured temperatures at the center of an image.

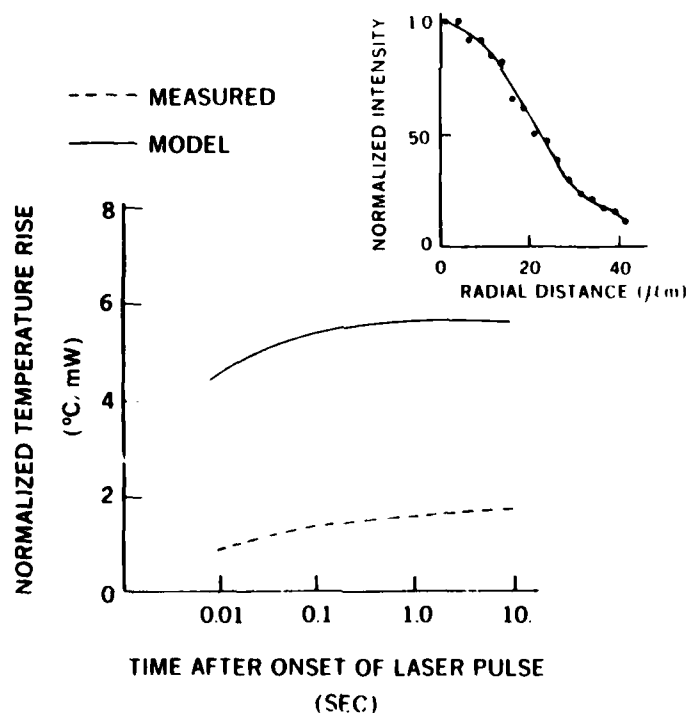


Figure 12. Temperature-rise history at the image center, normalized with respect to corneal power for a 9.0-sec exposure. Retinal irradiance profile is shown in the insert (Polhamus: Ref. 22).

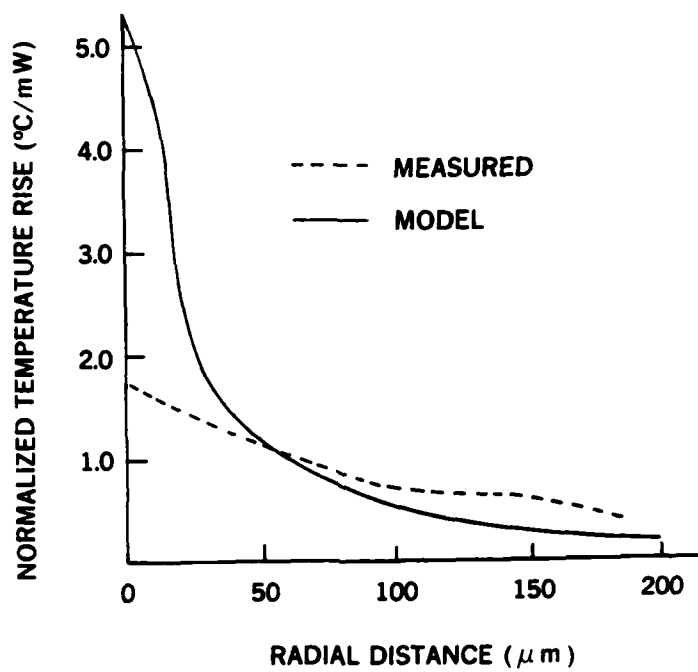


Figure 13. Radial temperature rise profiles at 9.0 sec, normalized with respect to corneal power (Polhamus: Ref. 22).

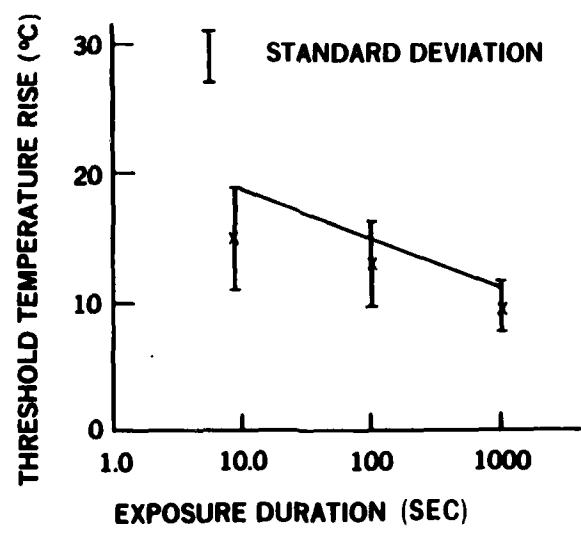


Figure 14. Maximum temperature rise at the lesion radius for combined macular and paramacular thresholds for various exposure durations. The predicted threshold temperatures, using parameters recommended by Takata et al. (Ref. 10), are represented by the solid line; and the mean measured threshold temperature, by an x.

Blood Flow

Eichler et al. (23) tested the significance of blood flow on tissue temperature profiles in the late 1970's. Using several different visible wavelengths of laser radiation, they radiated living and dead tissue while measuring steady-state temperature rise as a function of depth. Only a 10% difference was found in the temperature rise between live tissue being supplied with blood and dead tissue. Shortly thereafter, Welch et al. (24) used a dimensionless solution of the retinal temperature model to determine that, for exposures of less than 8 sec, blood perfusion reduced temperature rise by only 10%. Therefore, the prediction of retinal temperature rise and injury could safely neglect the effects of blood flow.

Asymptotic Retinal Thermal Injury

The thermal model is normally solved numerically; however, the asymptotic nature of the solution lends itself to a graphical approach. To predict damage, one need only determine the energy required to produce a "threshold" temperature rise profile at a given lesion radius. That threshold temperature rise is one which will, when subjected to Henriques' damage integral, predict irreversible injury. The threshold exposure is then:

$$Q_t = T_t / V_r A \quad (16)$$

for

Q_t = threshold retinal exposure (J/cm²)

T_t = threshold temperature rise at the lesion radius (°C)

V_r = normalized temperature rise at the lesion radius (°C/J)

A = aperture area of 7-mm pupil = 0.38 cm².

In the absence of a plot of normalized radial temperature profiles from Gaussian images from which to obtain V_r , minor modification to equation (16) yields:

$$Q_t = T_t R_r / V_c A \quad (16.1)$$

for the same definitions of Q_t , T_t , and A as for equation (16), and:

R_r = Ratio of temperature rise at the image center to that at the lesion radius

V_c = normalized maximum center temperature rise (°C/J).

Thus, to obtain the threshold temperature rise, use can be made of the asymptotic plot--by Priebe and Welch (25)--of the lesion radius threshold temperatures (T_t) shown in Figure 15. Figure 15 was derived with rate coefficients obtained from porcine skin burns. Another set of damage coefficients can be those already mentioned, generated from the data of Figure 14; however, the difference between the two sets is only 5%. The plot shows the maximum temperature at the radius for irreversible injury ($\omega = 1$, for this plot). For instance, the maximum temperature at the lesion radius for a 1-ms threshold exposure is 33°C. Using an assumed image size of 25 μm $1/e^2$ radius, Priebe and Welch generated this curve with experimental threshold data from the literature.

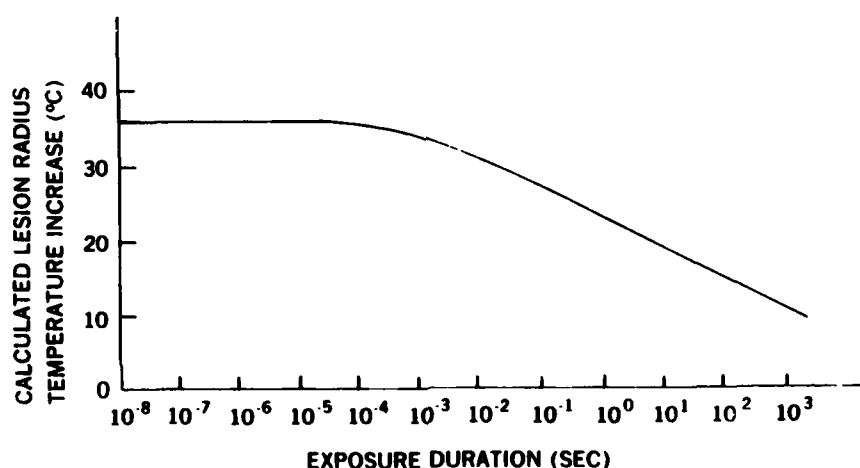


Figure 15. Asymptotically predicted threshold temperatures at the lesion radius using the thermal model coupled with the rate process model--the coefficients in the rate process model are $A = 3.1 \times 10^{98} \text{ sec}^{-1}$ and $E = 150,000 \text{ cal mole}^{-1}$ (Priebe and Welch: Ref. 25).

Model solutions show that 40% changes in image size affect maximum temperature rise at the lesion radius by no more than 3% (26). We would expect this finding, since the exponential nature of the integrand in Henriques' rate process model makes the results highly sensitive to peak temperature instead of the general shape of the temperature-time profile.

The normalized temperature rise at the center of the image was tabulated by Mainster et al. (27), and Priebe and Welch (25) later emphasized its asymptotic nature (Fig. 16). The curves of Figure 16 were calculated by use of absorption coefficients of $\beta_1 = 1425 \text{ cm}^{-1}$ and $\beta_2 = 163 \text{ cm}^{-1}$, which are Coogan et al.'s values for $\lambda = 530 \text{ nm}$ (12). However, Figure 17 was obtained by use of $\beta_1 = 310 \text{ cm}^{-1}$ and $\beta_2 = 53 \text{ cm}^{-1}$ (27). Though the temperatures will be different due to different absorption coefficients (the center temperature from Fig. 16 for $2\sigma = 10\mu$ is 100 X larger than that of Fig. 17), the ratios of center to lesion radius temperature should be relatively unchanged. Model

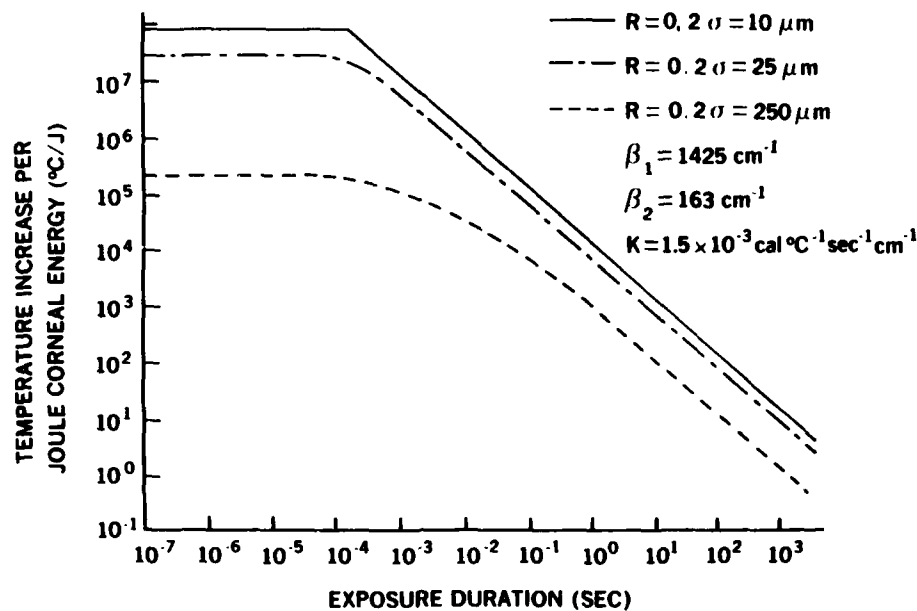


Figure 16. Temperature increase per joule total intraocular energy vs. exposure duration (Priebe and Welch: Ref. 25). Refer to Figure 18 for definition of σ .

calculations with $\beta_1 = 1108 \text{ cm}^{-1}$ and $\beta_2 = 145 \text{ cm}^{-1}$ (647 nm, by Coogan (12)) compared to those with $\beta_1 = 360 \text{ cm}^{-1}$ and $\beta_2 = 260 \text{ cm}^{-1}$ (647 nm, obtained using the transmission value of Gabel (9) and the thicknesses measured by Coogan (12)) show their ratios of center temperature to lesion radius temperature (averaged over exposures from 10^{-3} to 10^{-5} sec) differ only by 19% (Polhamus, G.D., unpublished data).

This analysis, and particularly the use of Figure 17, is valid only for small images ($\approx 10 \text{ } \mu\text{m}$ $1/e^2$ radius). To estimate threshold exposures from images larger than $10 \text{ } \mu\text{m}$ $1/e^2$ radius, the dependence of radial temperature profiles on image size must be known. Priebe and Welch (28) have normalized information for uniform profiles, as shown in Figure 18.

Using information from Figures 15, 16, and 17, threshold exposures for minimal image size were calculated and compared to literature data in Figure 19. The image was assumed to be either $25 \text{ } \mu\text{m}$ or $10 \text{ } \mu\text{m}$ $1/e^2$ in radius, and the minimum ophthalmoscopically visible lesion to be $12.5 \text{ } \mu\text{m}$ in radius. For the particular example of 1 ms, the threshold calculated by equation (16.1) was $2.9 \times 10^{-5} \text{ J/cm}^2$. The calculated values are about 50% below experimental data for 1 ms to 1000 sec, but approximately 40% above experimental data for exposures shorter than 0.1 ms.

This approach shows agreement between a model of thermal injury and the general trend of the experimental data between 10^{-8} and 10 sec exposure duration. Unfortunately, the model appears to be limited to single exposures, since Hemstreet et al. (29) showed that the model did not predict injury from multiple pulse exposures. Despite this limitation, a modified model has been used fairly successfully for the prediction of laser damage following single exposures of the cornea and skin.

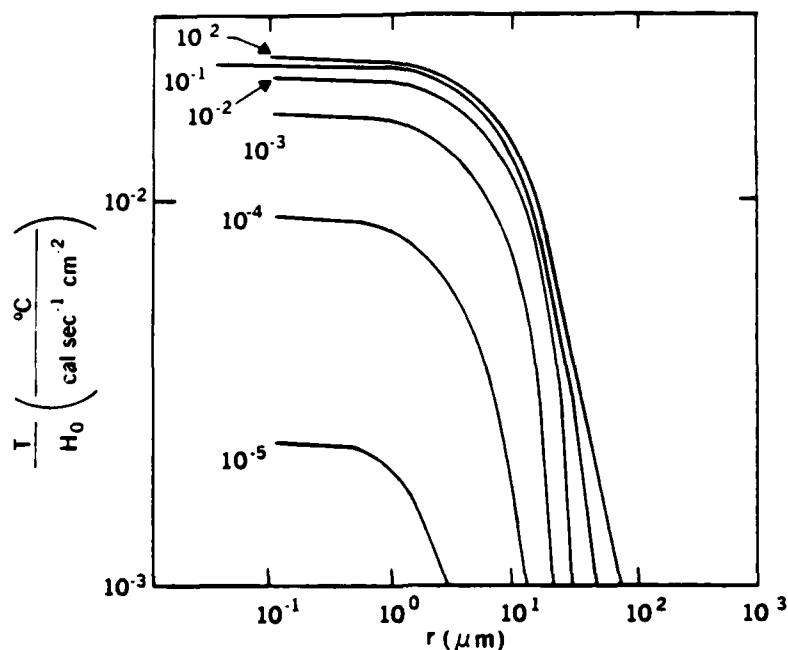


Figure 17. Normalized temperature for a constant exposure and the point-spread distribution associated with a 6.6-mm pupil diameter. Radial ($z=1 \mu\text{m}$) temperature distributions are given (Mainster et al.: Ref. 27).

CORNEAL THERMAL INJURY

In the far infrared (IR) region (i.e., for wavelengths greater than 1400 nm), the mechanism of interaction is generally considered to be thermal--at least at the threshold level; and effects are produced primarily in the cornea and lens, for very little energy is transmitted to the retina at these wavelengths. Although a minimal epithelial corneal lesion is not particularly significant in terms of a permanent effect on visual function, the production of stromal injury with associated edema and subsequent collagen shrinkage is viewed as serious, because extended or permanent loss of visual capacity can be involved--as shown by Gallagher (30).

Safety standards for corneal exposure to laser IR radiation have been developed on the basis of the production of a minimal epithelial corneal lesion, visible within about one hour, and with a slit lamp being used for the examinations. Typically, such a lesion would appear as a greyish cloudy area--a small opacity, or a "stippling" being located within the irradiated area. Maximum permissible exposure levels (MPE) were established by using a suitable safety factor, generally around ten, below the value of the exposure

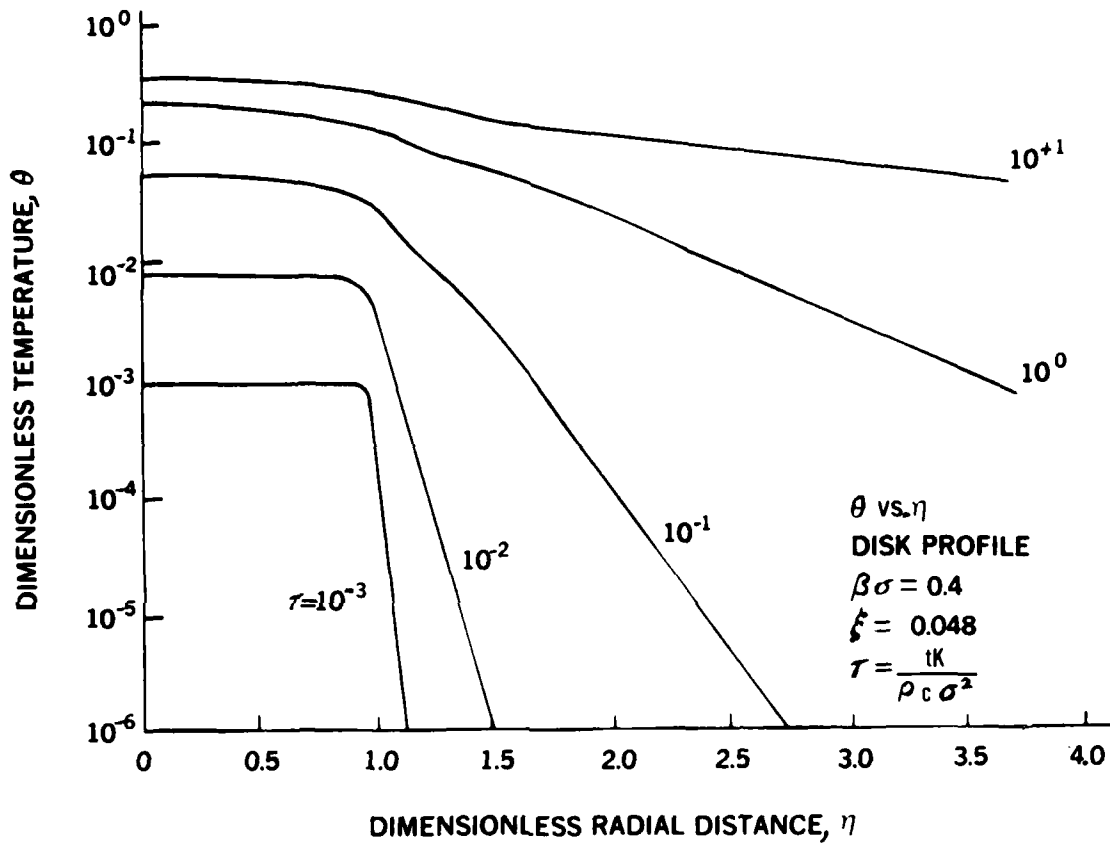


Figure 18. Dimensionless temperature vs. dimensionless radial distance for uniform irradiance profile. Here: $\theta = Tk/\beta H_0 \sigma^2$; $\eta = r/\sigma$; and $\xi = \beta z$; $T =$ temperature rise ($^{\circ}\text{C}$); $K =$ thermal conductivity ($\text{cal/cm} \cdot \text{s} \cdot ^{\circ}\text{C}$); $\beta =$ absorption coefficient at wavelength λ for a single layer of the retinal-choroid complex (cm^{-1}); $H_0 =$ center retinal spectral irradiance ($\text{cal/cm}^2 \cdot \text{s}$); $\sigma =$ radius of a Gaussian image at the $1/e$ point, or the radius of a uniform image; $r =$ radial distance in the image (cm); $z =$ axial distance (cm); $t =$ time (sec); and $Pc =$ volumetric specific heat ($\text{cal/cm}^3 \cdot ^{\circ}\text{C}$) (Priebe and Welch: Ref. 28).

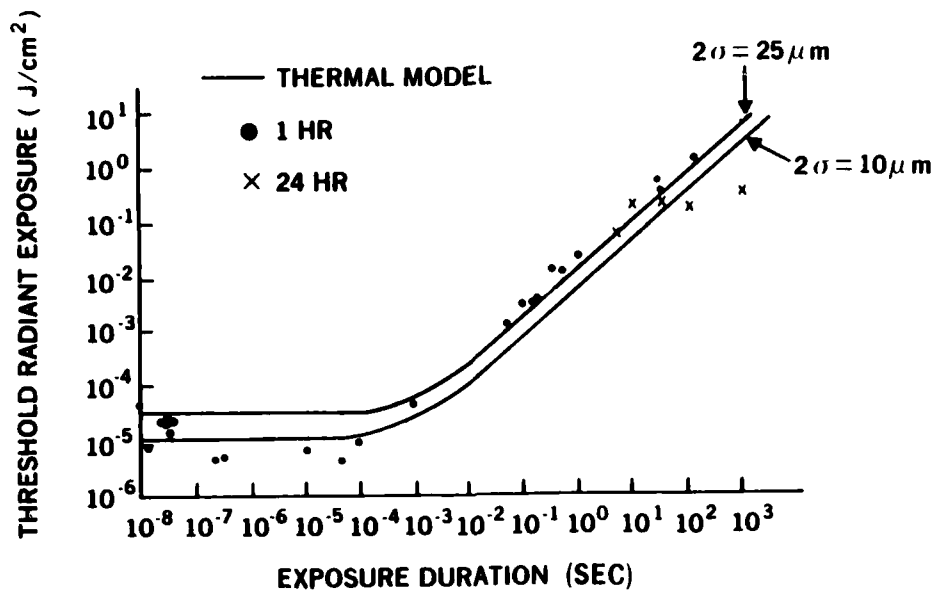


Figure 19. Model predictions for 25- and 10- μm image diameters compared to experimental observation of a minimum visible lesion of 25 μm $1/e^2$ diam. (with Henriques' rate constants).

(in terms of energy per unit area) that produced the minimal lesion. Although only a relatively small body of experimental data was available upon which to formulate standards, a well-developed understanding of thermal heating phenomena existed to guide and assist in estimating safe exposure levels. As a result, both of the wide range of wavelengths potentially producible by lasers in the IR region, and of the relatively broad and irregular IR absorption spectra of the cornea, aqueous, and lens, an ANSI standard was developed that was independent of wavelength in the spectral region of 1.4 to 10⁶ μm . This standard, which still applies, has only one exception: a wavelength of 1.5 μm --the wavelength produced by an erbium laser (Fig. 20).

The work by Gallagher (30) stimulated an interest in predicting different degrees of corneal injury. The retinal thermal model, structured to accommodate various layers of absorbing tissues, was rather easily adapted to calculating temperatures in the cornea and in the other clear media of the eye. Takata et al. (10) accomplished this adaptation in 1974 by introducing anatomical and physical properties appropriate to the various layers of the clear media (Fig. 21) in place of those for the retina and choroid (Table 2). This model assumed an air interface with the tear layer, but considered transfer of heat at this boundary only by conduction. From the work of Boettner (31) and Maher (32), absorption coefficients for the clear media were available (Fig. 22). This corneal model also included provision for injury assessment, using the Henriques damage assessment technique.

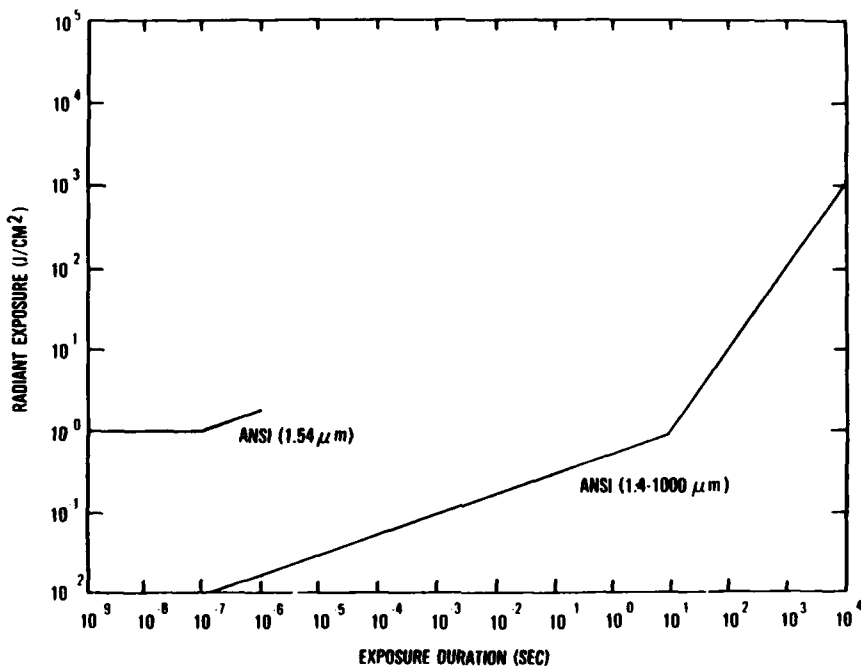


Figure 20. Safety standards for the cornea.

TABLE 2. PHYSIOLOGICAL PARAMETERS USED FOR CLEAR MEDIA ANALYSIS
(Takata et al.: Ref. 10)

<u>Ocular structures</u>	<u>Thicknesses (cm)</u>	
	Monkey	Man
Tear layer	6×10^{-4}	6×10^{-4}
Cornea	5.16×10^{-2}	5.86×10^{-2}
Aqueous humor	2.9×10^{-1}	3.1×10^{-1}
Lens	3.5×10^{-1}	3.6×10^{-1}
Vitreous humor	1.157	1.697
Pigment epithelium	1.2×10^{-3}	1.4×10^{-3}
Chorio-capillaris	1.0×10^{-3}	1.2×10^{-3}
Choroid	1.68×10^{-2}	1.42×10^{-2}
Sclera	1.0×10^{-1}	1.0×10^{-1}
Corneal surface to second principal plane	1.70×10^{-1}	1.75×10^{-1}
Corneal surface to pupil	2.9×10^{-1}	3.1×10^{-1}

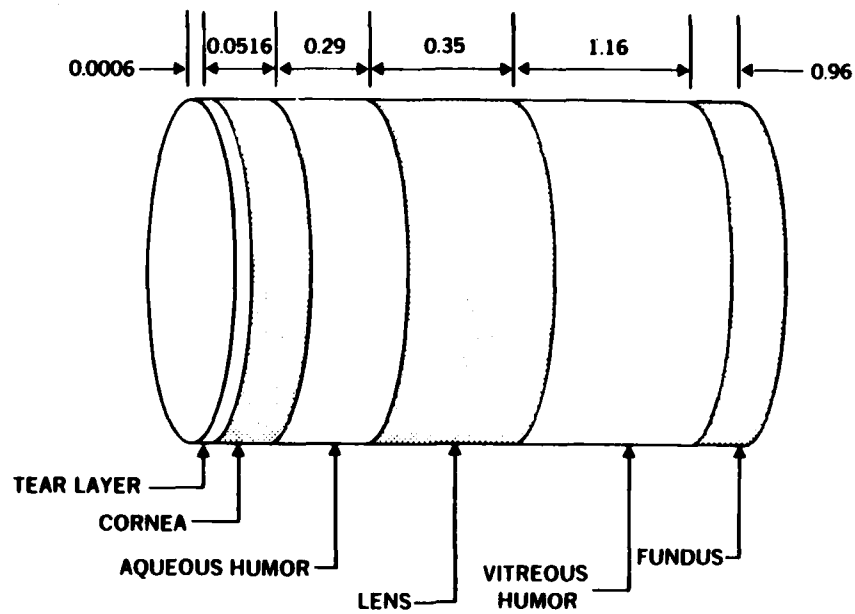


Figure 21. Cornea and lens model geometry (distances in centimeters).

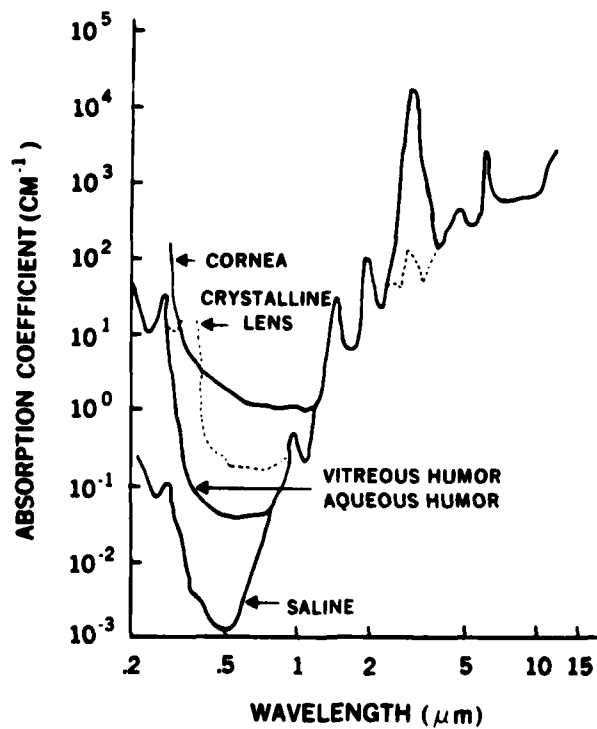


Figure 22. Absorption coefficients for the rhesus ocular media (Maher: Ref. 32).

In 1975-1977, Egbert and Maher (33) conducted an extensive analysis of the relationship between corneal injury "thresholds" experimentally determined and corneal temperature predictions in which the corneal thermal model was used. Egbert considered threshold production for three types of thermal corneal injury: (a) minimal epithelial lesion, defined as "the appearance of a relatively faint greyish-white stippled area within 1-2 hours"; (b) stromal opacity, observable as a clouding or an opacity within 1 hour postexposure; and (c) epithelial vaporization or perforation with severe stromal injury (crater formation, bubbles in the stroma, or perforation into the aqueous), observable immediately postexposure. He found that experimentally determined "thresholds"--more specifically, the exposure doses for which the probability for lesion formation was 50% (ED_{50})--for the various types of corneal injury could be fairly well characterized by a "critical peak temperature." From his calculations using the model, the various thresholds were found to vary inversely with the absorption coefficient at lower values of the absorption coefficients, but appeared to be independent of them for large values of the absorption coefficient; i.e., $>1000 \text{ cm}^{-1}$. He also observed that thresholds were independent of the radius of the incident beam for radii greater than about 10^{-2} cm . Further, for exposures less than about 10^{-3} to 10^{-4} sec , thresholds were independent of exposure durations. For exposure durations greater than about 1 sec, the thresholds appeared to be directly proportional to exposure duration.

In summary, Egbert and Maher (33) found the various threshold estimates made with the thermal model were within a factor of 0.3 to 10 of the mean experimental values. Of specific interest, he found calculations using the damage integral technique for epithelial lesion prediction were on the average within 3 percent of the average experimental value, and that 90 percent of these predictions were within a factor of two of the experimental values.

During 1976-78, Mikesell (34) examined the production and "repair" of corneal injury produced by CO_2 laser radiation ($10.6 \mu\text{m}$). In this study, he used Dutch-belted rabbits, and a continuous wave (CW) laser having a beam diameter at the $1/e$ point of 2.6 mm. All exposures were of 0.5 sec duration. He considered four types of injury: (a) minimum visible lesions observable with a bioslit lamp within 30 min of exposure; (b) visible lesions at specified times, up to 1 year; (c) changes in corneal curvature during the 1-year observation period; and (d) corneal heterogeneity (i.e., opacities or heterogeneous indices of refraction within the cornea). The results are summarized in Table 3 for the presence or absence of a visible lesion. He found that, with time, corneal curvature changes (measured in diopters) occurred in all groups (including the control group, as expected). Further, he found that these changes consisted of both decreased and increased corneal curvatures--including the exposed and control groups. However, the average change occurring in the exposed group showed a slow decrease, or flattening of the curvature, with time up to one year--with the most pronounced average flattening being associated with corneas that had received the higher exposures. The number of corneas showing changes greater than expected (relative to the control animals) was significant and the size of many of the measured changes indicated that significant effects on visual acuity could be expected.

TABLE 3. ED₅₀ VALUES OF AVERAGE POWER FOR CORNEAL LESIONS
AFTER EXPOSURE TO 10.6- μ m RADIATION

Postexposure time	Number of eyes	ED ₅₀ (watts)	95% Confidence limits
30 min	144	2.1	1.8 - 2.3
1 day	138	2.3	1.9 - 2.6
7 days	138	2.8	2.3 - 3.2
30 days	134	4.9	4.2 - 5.6
90 days	132	8.6	6.8 - 15.2
180 days	131	11.1	8.2 - 32.0
270 days	127	11.1	8.2 - 34.0
365 days	120	9.9	7.7 - 21.3

Laser beam radius = 2.65 mm at 1/e point.
Duration of all exposures = 0.5 sec.

Finally, using a hand-held ophthalmoscope to examine the fundus reflection for a lack of homogeneity, Mikesell (34) determined the threshold for corneal heterogeneity at 1 year to be 7.25 joules/cm². The measured thresholds for each type of injury were more than a factor of 10 above the corresponding ANSI maximum permissible exposure. Interestingly, the ratio of ED₅₀ for corneal heterogeneity to the ED₅₀ for a minimum visible lesion within 30 min was 1.5. If, as Mikesell recommends, the indication of permanent injury is taken as corneal heterogeneity at 1 year, the ED₅₀ for just visible corneal stippling, which is repairable within a day or two, is not far removed from that for permanent injury. However, the effect of corneal heterogeneity on visual function, as observed in these experiments, has not been shown.

On the bases of thermal models, Reed (35) and Vos (36) independently developed equations describing standards for eye safe exposures, in the IR region between 1.4 μ m and 10⁶ μ m, which take into account the wavelength dependence of energy absorption in the corneal tissues. Such a modification of the laser safety standards appears quite attractive, since the current standards do not consider the rather significant wavelength dependent effects.

Shown in Figure 23 are curves developed by Reed (35) predicting minimum epithelial corneal lesions, along with experimental data cited by Egbert and Maher (33). The two data points indicated by diamonds were obtained by Mueller and Ham (37) for CO₂ radiation, and correspond to the observation of light stippling at 48 hours postexposure--visible only with fluorescein staining of the cornea.

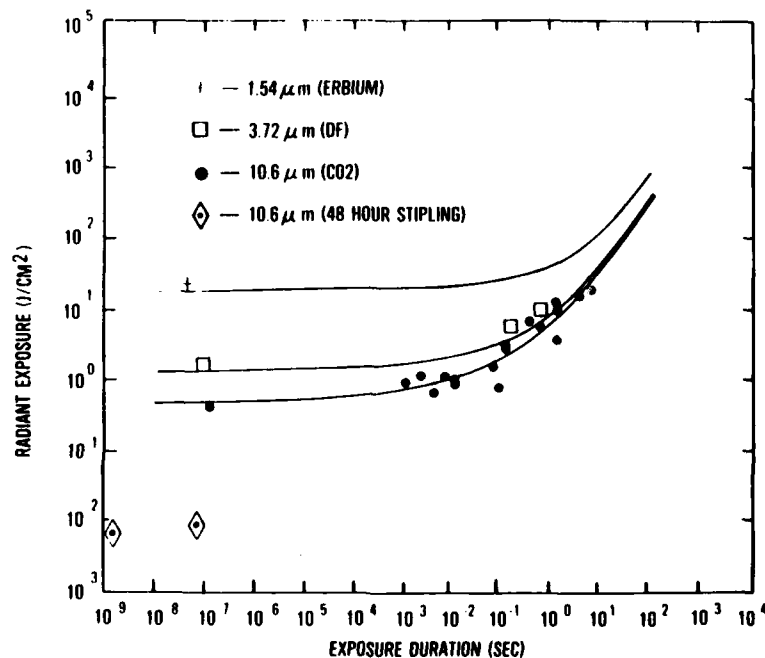


Figure 23. Comparison of experimental and theoretical (eq. 3) lesion thresholds for three absorption coefficients. Curves were developed by Reed (Ref. 35); and data points are as cited by Egbert and Maher (Ref. 33) for 10^{-8} - 10^2 sec.

Presented in Figure 24 are standards, as proposed by Reed (35), that can be compared with the current ANSI standard (Fig. 20). The two observations by Mueller and Ham (37) are also shown on Figure 24. Sliney (38) has taken the position that these two values may be the result of acoustic phenomena, or of some other mechanism operating at the very short exposure times involved. However, fluorescein uptake is known to be a more sensitive detector of injured tissue, especially 48 hours postexposure. Taboada et al. (39) found that detectable changes, when fluorescein had been used, could be observed at about one-twentieth of the dose that produced changes detectable without

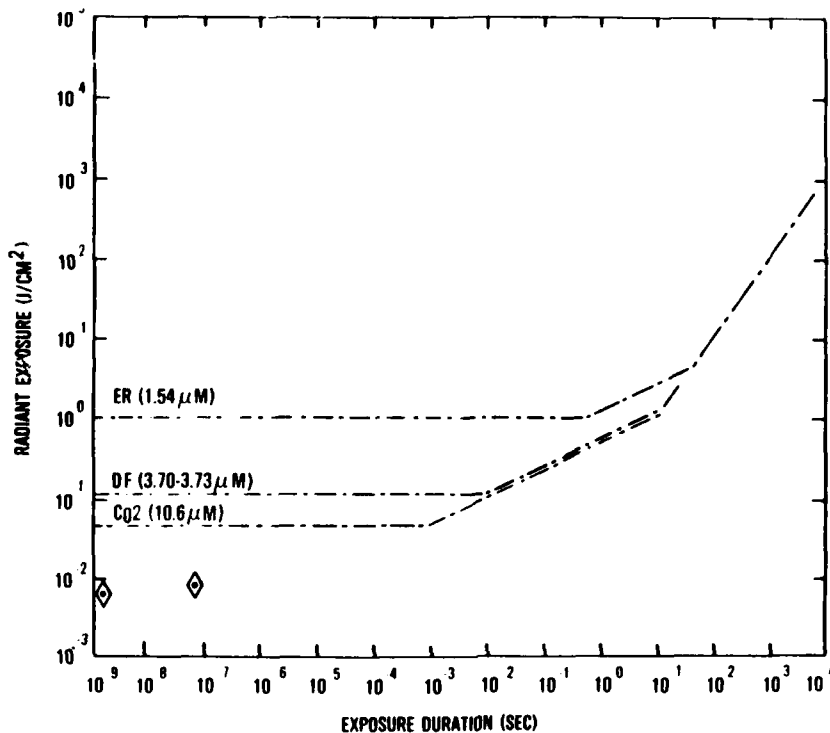


Figure 24. Proposed corneal safety standards (Reed: Ref. 35; and Vos: Ref. 36)

fluorescein at 2 hours postexposure for 248 nm, 50 ns radiation. In our view, had Mueller and Ham (37) employed the same criteria for a minimum epithelial lesion commonly used in most of the earlier work (i.e., the appearance of a light stippling or cloudiness within 1 hour--visible without staining), the threshold values would have been more nearly in line with other CO₂ data.

In any event, additional attention should be given to this portion of the spectrum, and revision of the IR standards should be considered, either to provide additional safety factors (as would be appropriate if the Mueller data were considered in the same light as previous "thresholds"), or to spread the standards with respect to wavelength, as has been done in the visible spectrum and as indicated appropriate by Vos (36), and in the Technical Report by Reed (35).

BEYOND THERMAL INJURY

In the last few years, research has shown a pure thermal model to have limited application for predicting injury. If exposures longer than a few seconds are involved, experimental evidence suggests a different mechanism of interaction--generally referred to simply as "photochemical," for want of a more definitive understanding of the detailed processes taking place. Undoubtedly a region exists in which the photochemical process is thermally moderated to some extent. Recognition of these findings has caused a lowering of the safety standards for prolonged exposures to visible light, and an introduction of a spectral dependence which reflects higher sensitivities of the retina as the wavelength approaches the blue end of the spectrum (Fig. 25). The evidence strongly suggests the photopigments of the detector cells are involved, and a photochemical process appears to be a likely candidate for the effects observed after low-level chronic exposures (40,41,42).

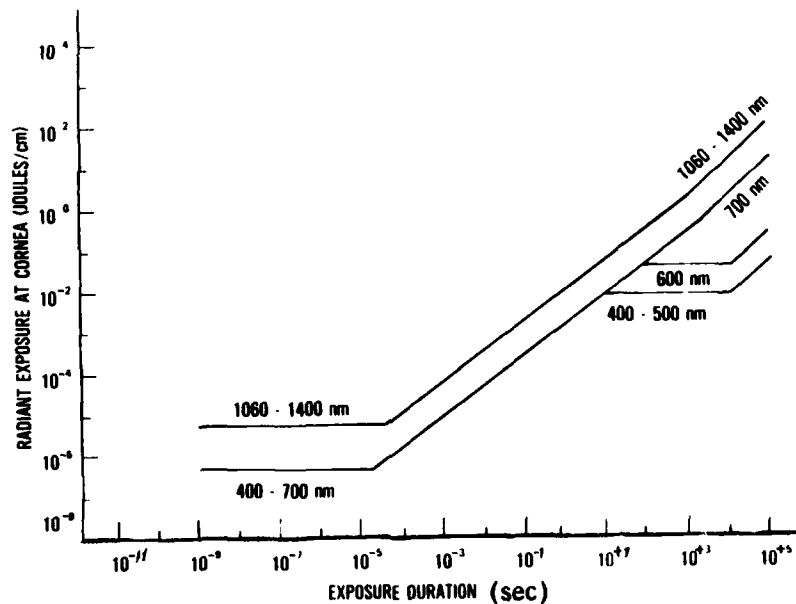


Figure 25. Safety standards for the retina.

At short exposures, of less than approximately 10^{-6} to 10^{-8} sec, another mechanism appears to become important. This mechanism is the production of acoustic transients which, if sufficiently large, can produce mechanical damage to the delicate retinal structures as well as the underlying choroidal tissues. Cleary, of the Medical College of Virginia, treated this subject in detail (43). Again, presumably, a region exists in which near-threshold injury is produced by a combination of thermal and acoustic effects.

Finally, when the retina is exposed to extremely high powers, such as can occur in extremely short pulses of less than about a nanosecond, new or different mechanisms (such as dielectric breakdown or multiple photon events) may occur. These mechanisms are generally reflected in a power-dependent relationship between threshold and exposure, rather than in an energy-dependent relationship, and are suspected to involve cellular membranes as well as other structures (44).

These nonthermal mechanisms apply to retinal effects which occur in the wavelength region between 400 and 1400 nm. As indicated earlier, primary effects produced by ultraviolet radiation occur in the cornea and lens. At 325 - 335 nm, however Zuclich and Taboada (45) observed retinal lesions (discolorations) at corneal exposures approximately a factor of 100 below the threshold for corneal effects observable with a slit lamp. Histological examinations implicate the detector cells carrying the photopigments--again suggesting a photochemical process. Although specific photochemical reactions may be difficult to identify, they should (in general) display a cumulative effect, obey reciprocity, and have a wavelength dependence with a long wavelength cutoff.

Briefly discussed has been possible ocular injury resulting from the interaction of radiant energy from "bright" lights of various wavelengths with varying parts of the eye. Listed in Table 4 are some of the bright light sources that can cause eye injury, and the possible consequences to vision.

CONCLUSION

Man's susceptibility to injury from intense light has required development of safety criteria--primarily for the retina, but also for the lens, cornea, and skin. Historically, investigators have developed retinal safety data for worst case situations on the basis of minimum visible type lesions (visible with an ophthalmoscope or slit lamp) and the estimated exposure for 50% probability of lesion occurrence within one hour--suitably adjusted with safety factors developed using the best information available at the time. This approach apparently was and is reasonable and appropriate for thermal and thermal-acoustic interactions. On the other hand, studies dealing with long exposures or low-level repeated exposures may require other endpoints and procedures. Active study of this subject is presently underway.

Current safety standards appear to be carefully conceived and based upon a large body of empirical information. As has been indicated, however, they are neither complete nor final, and do not explicitly consider potential effects on visual function, the possibility of accelerated retinal aging, or latent effects.

TABLE 4. BRIGHT LIGHT SOURCES AND SOME POSSIBLE CONSEQUENCES TO OVEREXPOSURE

<u>Source</u>	<u>Site of effect</u>	<u>Possible effects</u>	<u>Consequences</u>
Sun	Cornea (UV) Retina (visible)	Kerato conjunctivitis Solar retinal burn, flashblindness ^a	Pain, inflammation, recovery in 24-48 hours No pain, small scotoma, possibly some noticeable loss of visual acuity at high acuities for bilateral burns
Arc welder	Cornea (UV)	Kerato conjunctivitis	Pain, inflammation, recovery in 24-48 hours
Intense arc lights with glass envelopes (Xenon)	Retina (visible and near IR)	Retinal burn	No pain, small scotoma, possibly some permanent loss of visual acuity
Intense arc lights with no UV filtering envelope	Retina (visible and near IR)	Retinal burn	No pain, small scotoma, possibly some permanent loss of visual acuity
Ophthalmic surgical lamps	Corneal (UV)	Kerato conjunctivitis	Pain, inflammation, recovery in 24-48 hours
	Retina	Retinal burns	No pain, possible small scotoma, possible color response shift
Nuclear detonation	Retina	Retinal burn, retinal hemorrhage, flashblindness ^a	Effects may range from minor to severe, temporary or permanent, involving loss of visual acuity and scotomas
Lasers	Cornea (UV, IR)	Kerato conjunctivitis, epithelial cell injury, stromal cell injury	Effects may range from minor kerato conjunctivitis to severe stromal scarring and change of cornea's curvature with associated loss of visual acuity
	Lens (UV, IR)	Cataracts	Small opacities in the lens producing increased light scattering and/or obstructions to vision in the eye. Prompt or delayed cataractogenesis
	Retina (near UV, visible, Near IR)	Detector cell damage, retinal burn, retinal hemorrhage, neural damage	Effects on vision may range from no significant effect to permanent effects involving loss of visual acuity, scotomas, or shifts in color response
Photoflash bulbs	Retina	Flashblindness ^a	No permanent effects. Recovery from flashblindness: in a few seconds

^aFlashblindness, which may occur following exposure to any visible "bright" light, is a partial and temporary loss of visual function that can last from several seconds to minutes or hours, depending upon the extent of the exposure.

REFERENCES

1. Allen, R. G., et al. The Calculation of Retinal Burn and Flashblindness Safe Separation Distances. SAM-TR-68-106, Sept 1968.
2. Ham, W. T., Jr., H. Wiesinger, F. H. Schmidt, R. C. Williams, R. S. Ruffin, M. C. Schaffer, and D. Guerry III. Flash Burns in the Rabbit Retina. Am J Ophthalmol, Vol 46, pp 700-723, 1958.
3. Allen, R. G. Research on Ocular Effects Produced by Thermal Radiation. Report for the USAF School of Aerospace Medicine by Technology Incorporated, Life Sciences Division, San Antonio, Tex. (July 1967).
4. Richey, E. O., and N. E. Lof. Predicting Safe Distances To Prevent Retinal Burns from Nuclear Detonations. SAM-TR-75-30, Dec 1975.
5. Wray, J. L. Model for Prediction of Retinal Burns. Technical Staff Study, DASA 1282, Headquarters DASA, Washington, D.C., 1962.
6. Vos, J. J. A Theory of Retinal Burns. Bull Math Biol, Vol 24, p 115, 1962.
7. Clarke, A. M., W. J. Geeraets, and W. T. Ham, Jr. An Equilibrium Thermal Model for Retinal Injury from Optical Sources. Appl Optics, Vol 8, No 5, May 1969.
8. Mainster, M. A., T. J. White, and R. G. Allen. Spectral Dependence of Retinal Damage Produced by Intense Light Sources. J Opt Soc Am, Vol 6, June 1970.
9. Wissler, E. H. An Analysis of Chorioretinal Thermal Response to Intense Light Exposure. IEEE Trans Biomed Eng, Vol BME-23,3, pp 207-215, 1976.
10. Takata, A. N., et al. Thermal Model of Laser Induced Eye Damage. Final Technical Report, Illinois Institute of Technology, Research Institute (IITRI), J-TR-74-6324, Oct 1974.
11. Henriques, F. C. Studies of Thermal Injury. Arch Pathol, Vol 43, p 489, 1947.
12. Coogan, P. S., W. F. Hughes, and J. Mollsen. Histologic and Spectrophotometric Comparisons of the Human and Rhesus Monkey Retina and Pigmented Ocular Fundus. Final Report of USAF School of Aerospace Medicine Contract AF41609-71-C-0006, Jan 1974.
13. Gabel, V. P., R. Birngruber, and F. Hillenkamp. Light Absorption in the Fundus of the Eye. Munich, Germany: Munich University Press, 1976.
14. Flamant. Repartition Dans l'Image Retinienne d'une Fente. Rev d'Optique, Vol 34, p 9, Sept 1955.
15. Westheimer, G., and F. W. Campbell. Light Distribution in the Image Formed by the Living Human Eye. J Opt Soc Am, Vol 52, p 879, Nov 1954.

16. Campbell, F. W., and R. W. Gubisch. Optical Quality of the Human Eye. *J Physiol*, Vol 186, p 558, 1966.
17. Robson, J. G., and C. Enroth-Cugell. Light Distribution in the Cat's Retinal Image. *Vision Res*, Vol 18, pp 159-173, 1978.
18. Polhamus, G. D., R. G. Allen, and K. Schepler. In-Vivo Measurement of the Point Spread Function in the Rhesus Monkey. *Proc 32nd Conf Eng'g in Med and Biol*, Denver, Colo., Vol 21, p 144, 1979.
19. Johnson, F. H., H. Eyring, and B. J. Stover. *Theory of Rate Process in Biology and Medicine*. New York: John Wiley and Sons, Inc., 1974.
20. Cain, C. P., and A. J. Welch. Thin Film Temperature Sensors for Biological Measurements. *IEEE Trans Biomed Eng*, Vol 21, No 4, pp 421-423, 1974.
21. Priebe, L. A., C. P. Cain, and A. J. Welch. Temperature Rise Required for Production of Minimal Lesions in the Macaca Mulatta Retina. *Am J Ophthalmol*, Vol 79, pp 405-413, 1975.
22. Polhamus, G. D. In-Vivo Measurement of Long-term Laser Induced Retinal Temperature Rise. *IEEE Trans Biomed Eng*, Vol 27, pp 617-622, 1980.
23. Eichler, J., J. Knof, H. Lenz, J. Salk, and G. Schafer. Temperature Distribution in Tissue During Laser Irradiation. *Rad Environ Biophys*, Vol 15, pp 277-287, 1978.
24. Welch, A. J., E. H. Wissler, and L. A. Priebe. Significance of Blood Flow in Calculations of Temperature in Laser Irradiated Tissue. *IEEE Trans Biomed Eng*, Vol BME-27, pp 164-166, 1980.
25. Priebe, L. A., and A. J. Welch. Asymptotic Rate Process Calculations of Thermal Injury to the Retina Following Laser Irradiation. *J Biomech Eng*, Vol 100, pp 49-54, 1978.
26. Welch, A. J., L. A. Priebe, L. D. Forster, R. G. Gilbert, C. Lee, and P. Drake. Experimental Validation of Thermal Retinal Models of Damage from Laser Radiation. Final Report for USAF School of Aerospace Medicine Contract F33615-76-C-0605, 1978.
27. Mainster, M. A., T. J. White, J. H. Tips, and P. W. Wilson. Retinal-Temperature Increases Produced by Intense Light Sources. *J Opt Soc Am*, Vol 60, pp 264-270, 1970.
28. Priebe, L. A., and A. J. Welch. A Dimensionless Model for the Calculation of Temperature Increase in Biologic Tissues Exposed To Nonionizing Radiation. *IEEE Trans Biomed Eng*, Vol 26, pp 244-250, 1979.
29. Hemstreet, H. W., Jr., J. S. Connolly, and D. E. Egbert. Ocular Hazards of Picosecond and Repetitive-Pulsed Lasers. Vol I: Nd:YAG Laser (1064 nm). SAM-TR-78-20, Apr 1978.

30. Gallagher, J. T. Corneal Curvature Changes Due To Exposure to a Carbon Dioxide Laser: A Preliminary Report. SAM-TR-75-44, Dec 1975.
31. Boettner, E. A. Spectral Transmission of the Eye. Final Report on USAF School of Aerospace Medicine Contract AF 41 (609)-2966, Jul 1967.
32. Maher, E. F. Transmission and Absorption Coefficients of Ocular Media of the Rhesus Monkey. SAM-TR-78-32, Dec 1978.
33. Egbert, D. E., and E. F. Maher. Corneal Damage Thresholds for Infrared Laser Exposure: Empirical Data, Model Predictions, and Safety Standards. SAM-TR-77-29, Dec 1979.
34. Mikesell, G. W., Jr., E. O. Richey, J. Taboada, R. C. McNee, B. R. Anderson, and J. L. Bower. Lesion Duration and Curvature Change in the Cornea Following Exposure to a Carbon Dioxide Laser. SAM-TR-79-26, Oct 1979.
35. Reed, R. D. Format of Revised Safety Standards for Infrared Laser Exposure. SAM-TR-78-29, Oct 1978.
36. Vos, J. J. Personal Communication, Apr 1978.
37. Mueller, H. A., and W. T. Ham, Jr. The Ocular Effects of Single Pulses of 10.6 μm and 2.5 - 3.0 μm Q-switched Laser Radiation. USAF School of Aerospace Medicine Report to the Los Alamos Scientific Laboratory, L-Division, Los Alamos, N.M., 1976.
38. Sliney, D. H. Personal Communication, Apr 1978.
39. Taboada, J., G. W. Mikesell, Jr., and R. D. Reed. Response at the Corneal Epithelium to Kr F Excimer Laser Pulses. Health Physics (In press).
40. Gibbons, W. D., and R. G. Allen. Retinal Damage from Long-term Exposure to Laser Radiation. Invest Ophthalmol Vis Sci, Vol 16, p 6, 1977.
41. Ham, W. T., et al. Sensitivity of the Retina to Radiation Damage As a Function of Wavelength. Photochem Photobiol, Vol 29, pp 735-743, 1979.
42. Harwerth, R. S., and H. G. Sperling. Prolonged Color Blindness Induced by Intense Spectral Lights in Rhesus Monkey. Science, Vol 174, pp 520-523, 1971.
43. Cleary, S. G. Laser Pulses and the Generation of Acoustic Transients In Biological Material. Laser Applications in Medicine and Biology, Vol 3, Ch 2. New York: Plenum Press, 1977.

44. Taboada, J., and R. W. Ebbers. Ocular Tissue Damage Due To Ultrashort nm Light Pulses from a Mode-locked Nd:glass Laser. Appl Optics, Vol 14, pp 1759-1769, Aug 1975.
45. Zuclich, J. A., and J. Taboada. Ocular Hazard from UV Laser Exhibiting Self-modelocking. Appl Optics, Vol 17, pp 1482-1484, 1978.